Coulomb effect in Au+Au and Pb+Pb collisions as a function of collision energy

D. Cebra, S.G. Brovko, C.E. Flores
University of California - Davis, Davis, California 95616

B.A. Haag
American River College, Sacramento, California 95841

J.L. Klay
California Polytechnic State University, San Luis Obispo, California 93407

(Dated: August 7, 2014)

The subtle differences between positive and negative pion spectra can used be used to study the nature of the nuclear interaction region in heavy-ion collisions. Several large acceptance heavy ion experiments at facilities ranging from SIS, the AGS, the SPS, to RHIC have measured mid-rapidity π^+ and π^- spectra for central Au+Au or Pb+Pb collisions. From these spectra one can create pion ratios as a function of $m_t - m_0$, which are used to determine the Coulomb potential, V_C, and the initial pion ratio, R_i, across a range of collision energies from 1 to 158 AGeV. The implications of the V_C and R_i trends with collision energy will be discussed.

PACS numbers: 25.75.-q, 25.75.Dw

arXiv:1408.1369v1 [nucl-ex] 6 Aug 2014

I. INTRODUCTION

In heavy-ion collisions, the subtle structure of the pion spectra can be used to image the positive charge density of the expanding fireball. The source has a net positive charge from the incident protons in the projectile and target. The Coulomb force resulting from this net charge accelerates each charged particle emitted from the source, and in doing so changes its final (observed) energy. Positively charged particles get a modest increase in kinetic energy while negatively charged particles are reduced. For the purposes of this paper, it is assumed that the 'initial-state' consists of particles that are emitted from a thermally equilibrated volume that has reached chemical and kinetic freeze-out; the Coulomb interaction is considered to be a 'final-state'interaction. These final-state Coulomb interactions distort the initial thermal spectra. This distortion can best be observed by comparing spectra of particles with the same mass but opposite charge. The effect is greatest for the lightest particles, the pions. The magnitude of the boost or reduction in kinetic energy is proportional to the Coulomb potential, V_C, which is determined by the charge distribution of the source and the emission point of the pion. Thus by studying the details of the pion spectra, one can effectively image the charge density of the source at kinetic freeze-out.

A relative enhancement, at low transverse momentum, of the negative pion yield with respect to that of the positive pions was first observed in heavy-ion experiments at the Bevalac [1–4]. These early results were explained as evidence of the positive Coulomb potential of the source. A similar enhancement of π^-'s at low m_t ($m_t = \sqrt{p_t^2 + m^2}$) was observed in silicon-induced heavy-ion reactions at the Alternating Gradient Synchrotron (AGS) [5, 6]. Early theoretical work [7–12] described these results in terms of emission from a static Coulomb source. Interpretation of these results is confounded by the difficulties in determining the impact parameter, source velocity, and source size in asymmetric heavy-ion collisions.

Pion spectra and ratios have been measured in symmetric collisions of the heaviest nuclei (Au+Au and Pb+Pb) at facilities ranging from SIS [13–15], the AGS [16–20], the SPS [21–28], to RHIC [29]. Several groups have analyzed the pion ratios to study the effect of the Coulomb potential. The KaoS group (at SIS) used a static model to analyze their mid-rapidity pion ratio data from 1 AGeV Au+Au collisions. They concluded that, in general, the freeze-out radius is a function of pion energy with the high energy pions freezing out first [14]. In a second study of the same data, they found the 'initial' pion ratio, R_i, to be 0.515 ± 0.05, and the V_C to be greater than 20 MeV [30]. A similar analysis of the E866 mid-rapidity 10.8 AGeV Au+Au data [16] found $R_i = 0.83$ and $V_C = 9 \pm 3$ MeV. This beam energy dependence is not unexpected.

The overall pion ratio is heavily influenced by the isospin asymmetry at low energy. As one increases the energy available for pion production, this ratio should approach unity. The Coulomb potential is a function of both the charge of the system and the source radius. The net charge of the interaction region is determined by the number of participant protons in the overlap volume of the projectile and the target and the degree of baryon stopping at a given bombarding energy. The observed decrease in V_C with beam energy is therefore indicative of either expansion or of a reduction in baryon stopping. These trends should be compared to the results from E877, an experiment in which pion ratios are studied at beam rapidity and higher. They find values of the 'overall' pion ratio, $R' = 1.09\pm0.20$ and $V_C = 31\pm22$ MeV [19]. The distinction between the 'initial' pion ratio, R, and the 'overall' pion ratio R' will be discussed later in this paper. Mid-rapidity pion ratio data are also

available from the top energy at the SPS. NA44 has reported pion ratios which showed evidence of a Coulomb effect [21]. WA98 reported pion ratios which are consistent with a finite Coulomb potential [22, 23]. They followed up this study with a more extensive analysis in which they related the source potential to the freeze-out time [24]. NA49 has studied pion ratios in peripheral collisions [31]; these results are explained in terms of isospin effects, time of initial pion emission, size of the pion source, and the Coulomb force [32].

Theoretical analyses were developed to include the Jacobian factor, d^3p_i/d^3p, [33], and the effects of radial expansion and pion emission time [34–37]. Ref. [36] concluded that: the SIS data are consistent with $V_C = 27$ MeV corresponding to a freeze-out radius of 8 fm, the AGS data are consistent with a radius of 10 fm, and the early SPS data (NA44) are consistent with a 9 fm radius. A full transport model calculation [38, 39] was also applied to these data. In that analysis, the freeze-out radius was also found to be 10 fm for the AGS and SPS data sets. Pion emission in heavy-ion collisions in the region 1 A GeV is investigated in an isospin dependent quantum molecular dynamics model in ref [40]. This analysis demonstrates that in this energy range pions are produced mostly through the Δ and $^*N$ channels.

In summary, for experimental mid-rapidity data, the Coulomb potential is observed to decrease with bombarding energy while the pion ratio rises. The theoretical analyses suggest an increase in freeze-out radius, which would correspond to a reduction in V_C, for beam energies from 1 to 10.8 AGeV.

In this paper, we review and analyze a range of available experimental data. We focus specifically on the low $m_t - m_0$ (< 0.3 GeV/c^2) region, as this is where the Coulomb potential has the biggest influence on the spectra and the ratios. We specifically have looked for data sets which extend to the lowest m_t; this allows a more detailed study of the effect of expansion on the slow pions. We have not considered data for collision energies below 1 AGeV. Although the threshold for inelastic nucleon-nucleon collisions is 0.3 GeV, the cross sections for the various $N+N \rightarrow N+\pi$ reactions rise rapidly from 0.3 before saturating at 1.0 GeV [41]. Also, we will not present results from bombarding energies above 158 AGeV. Although there are a wealth of spectra data from RHIC and the LHC, the degree of baryon stopping is very low at these higher energies, resulting in a very small Coulomb potential which would only be seen at the lowest end of the $m_t - m_0$ spectra. None of the RHIC or LHC experiments have especially low $m_t - m_0$ thresholds, therefore it is not possible to extract meaningful Coulomb potentials from those data.

II. RESULTS

Figure 1 shows the transverse mass spectra at mid-rapidity for both positive and negative pions from central Au+Au or Pb+Pb collisions at beam energies from 1 to 42 AGeV (references are given in the figure caption). We note that 42 AGeV is the fixed-target equivalent energy to the $\sqrt{s_{NN}} = 9.2$ GeV test run at RHIC from which $\pi^{\pm}$ spectra were published by the STAR Collaboration [29]. We also note that several energies which were studied at the SPS are not represented in this figure. Although NA49 has published π^- spectra at 40, 80, and 158 AGeV [27], they have not published π^+ spectra at these energies. WA98 has published pion ratios at 158 AGeV, however they too have only shown their π^- spectra. NA44 has shown both π^- and π^+ spectra at 158 AGeV, however their acceptance slice only allows low $m_t - m_0$ pions away from mid-rapidity. Although the positive and negative pion spectra are very similar in slope for $m_t - m_0 > 0.1$ GeV/c^2, a clear difference in the shape of the respective spectra is evident below 0.1 GeV/c^2 for all beam energies. In reference [20], the pion spectra were fit with the superposition of two independent Boltzmann distributions. The two contributions were interpreted to approximately represent the pion yields coming from Δ resonance decays (low temperature component) and from direct thermal emission of pions (high temperature component). Studies with RQMD [42] supported this general interpretation. The high temperature parameter was required to be the same for both the negative and positive pions for each beam energy. However, the low temperature parameter was determined independently.

In this paper, we address the details of the low $m_t - m_0$ shapes and amplitudes of the π^+ and π^- spectra in terms of the Coulomb potential from an expanding source. This interpretation of the pion spectra does not contradict the previous studies [20, 42]. The fact that the low m_t pions are predominantly daughters of Δ resonance decays [13, 43, 44] explains the difference in the relative yields of the two charges of pions. However, Δ resonance production does not explain the difference in spectral shapes. The Coulomb interaction modifies the initial spectral shapes as we show in this paper.

In the analysis outlined here, the shapes of the initial spectra (i.e. at hadronic freeze-out) are assumed to have been the same for both the positive and negative pions, however the initial yields of the two charges are different. The ratio of the initial yields is the 'initial' pion ratio R_i. After freeze-out, the final-state Coulomb interaction modifies the initial spectra, resulting in the final spectra. The final energy ($E_f = m_t \cosh y$) is related to the initial energy (E_i) through the addition/subtraction of the Coulomb potential (V_C) for the positive/negative pions:

$$E_f = E_i \pm V_C \tag{1}$$

The result is now an energy dependent final pion ratio ($R_f(E_f)$). For a static spherical source, including the proper Jacobian [33], $(E_f \pm V_C)\sqrt{(E_f \pm V_C)^2 - m^2}$, the

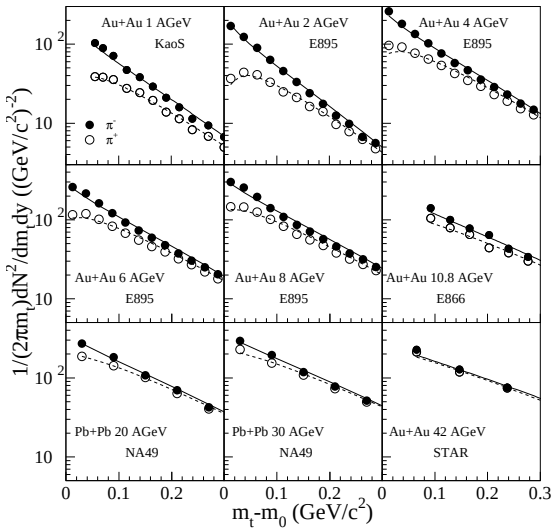

FIG. 1. The mid-rapidity $m_t - m_0$ spectra are shown for negative (solid symbols) and positive (open symbols) pions from central Au+Au and Pb+Pb collisions at 1.0 [14], 2.0 [20], 4.0 [20], 6.0 [20], 8.0 [20], 10.8 [16], 20 [28], 30 [28], and 42 [29] AGeV. The Coulomb distortion is exhibited by the divergence of the spectra at low $m_t - m_0$. The spectra are fit with a Bose-Einstein function modified by Coulomb acceleration due to the effective potential from Eqn. (4). A single temperature parameter is used at each bombarding energy to simultaneously fit the π^- (solid) and the π^+ (dashed).

final pion ratio as a function of E_f is given by:

$$R_f(E_f) = \frac{E_f - V_C}{E_f + V_C} \frac{\sqrt{(E_f - V_C)^2 - m^2}}{\sqrt{(E_f + V_C)^2 - m^2}} \frac{n^+(E_f - V_C)}{n^-(E_f + V_C)} \tag{2}$$

where the $n^{\pm}(E)$ are the pion emission functions describing the initial $\pi^{\pm}$ spectrum. In general, the pion emission functions in heavy-ion collisions are best represented by a Bose-Einstein distribution, so that:

$$\frac{n^+(E_f - V_C)}{n^-(E_i + V_C)} = \frac{A^+(e^{(E_f+V_C)/T_\pi} - 1)}{A^-(e^{(E_f-V_C)/T_\pi} - 1)} \tag{3}$$

where T_π is the slope parameter and the $A^{\pm}$ are the amplitudes characteristic of the initial pion distributions. The initial pion ratio, R_i, is defined as A^+/A^-. In reference [19], E877 replaced Eqn. (3) with a constant 'overall' pion ratio, R'. If one assumes a Maxwell-Boltzmann distribution for the initial pion spectra, then $R' = R_i e^{2V_C/T_\pi}$. However, using a Bose-Einstein form for the initial pion spectra results in an energy dependent emission function ratio, $n^+(E_f - V_C)/n^-(E_i + V_C)$, that can not be approximated with a constant R'.

The assumption of a static source is not valid for heavy-ion collisions. During the course of the interaction, the protons, which carry the bulk of the source charge, are emitted simultaneously with the pions. Thus the charged source is expanding during the course of the Coulomb interaction. Therefore, the low momentum pions do not experience the full Coulomb potential but rather a reduced potential. This reduced Coulomb potential, as a function of pion momentum, can be calculated by integrating the proton emission function up to a maximum kinetic energy corresponding to the pion velocity, $E_{\max} = \sqrt{(m_p p_\pi / m_\pi)^2 + m_p^2} - m_p$. Assuming that the proton emission function is given by a Maxwell-Boltzmann distribution with a characteristic slope parameter T_p, the effective Coulomb potential is:

$$V_{\text{eff}} = V_C(1 - e^{-E_{\max}/T_p}) \tag{4}$$

The mid-rapidity pion ratios for beam energies 1 to 158 AGeV are shown in Fig. 2 (references to the experimental data are given in the figure caption). The data are fit to the ratio function as given in Eqn. (2). The two curves in each panel correspond to either a fixed V_C or a V_{eff} given by Eqn. (4). For these fits, we have fixed the slope parameters of the pion and proton initial distributions to the values given in Table I. The pion initial slope parameters were fixed by simultaneously fitting the π^+ and π^- spectra in the range $0 < m_t - m_0 < 0.5$ GeV/c^2 to Coulomb-modified Bose-Einstein distributions.

$$\frac{1}{2\pi m_t} \frac{d^2N}{dy dm_t}(E_f) = (E_f \mp V_{eff}) \frac{\sqrt{(E_f \mp V_{eff})^2 - m^2} A^{\pm}}{(e^{(E_f \mp V_{eff})/T_\pi} - 1)} \tag{5}$$

where $E_f = m_t \cosh y$, $A^{\pm}$ is a normalization constant, and V_{eff} is given by Eqn. (4). These fits are shown by the solid (π^-) and dashed (π^+) curves in Fig. 1. The pion slope parameters used in this analysis are lower than those reported previously [14, 16, 20] at each beam energy because this analysis focuses on the $m_t - m_0$ region below 0.5 GeV/c^2, whereas the published slope parameters come from fits to higher $m_t - m_0$ regions of the spectra. The proton slope parameters given in Table I were determined using Maxwell-Boltzmann fits to spectra data from previous publications [26, 45–53]. For this analysis, the fit range was limited to $0.25 < m_t - m_0 < 1.0$ GeV/c^2. The slope parameters used in this analysis are similar to those cited by the authors of the original studies.

The fits to the pion ratio data in Fig. 2 were achieved with two free parameters, the Coulomb potential, V_C, and the initial pion ratio, R_i. It is evident that the low $m_t - m_0$ data points are better fit by the effective potential (solid curve) than by a fixed V_C (dashed curve). The magnitude of the correction due to the effective Coulomb potential of Eqn. (4) is determined by the proton slope

TABLE I. T_π and T_p are slope parameters describing the pion and proton spectra. These are fixed parameters in the fits to the pion ratio data using Eqn. (2) with the effective Coulomb potential given in Eqn. (4). These fits are shown by the solid curves in Fig. 2. The extracted Coulomb potential (V_C) and initial pion ratio (R_i) are tabulated for each bombarding energy.

$E_{\rm beam}$ (AGeV)	T_π (MeV)	T_p (MeV)	$V_C\|_{y=0}$ (MeV)	$R_i\|_{y=0}$
1	75	172	27.8 ± 1.3	0.469 ± .011
2	81	183	24.8 ± 0.9	0.515 ± .005
4	86	203	21.9 ± 0.5	0.639 ± .004
6	92	216	19.3 ± 0.4	0.694 ± .004
8	94	225	17.5 ± 0.5	0.710 ± .004
10.8	100	229	16.5 ± 4.1	0.749 ± .035
20	104	234	13.3 ± 3.0	0.834 ± .008
30	119	243	8.8 ± 1.5	0.871 ± .009
42	125	252	8.2 ± 5.0	0.950 ± .050
158	130	257	7.9 ± 0.5	0.930 ± .003

parameter. To test our assumptions, we have allowed the proton slope parameter to be a third free parameter. In these cases we found T_p to be consistently 30-50 MeV greater than the published values. This systematic discrepancy comes from the radial flow of the protons [54]. The Maxwell-Boltzmann distribution which was used to fit the proton spectra does not include the effect of radial flow and consistently overestimates the proton spectra at low $m_t - m_0$. The pions are sensitive to the lower energy range and as a result a higher proton slope parameter is suggested. We note that using the $V_{\rm eff}$ in the fits increases the V_C required to match the observed results. Therefore, our extracted values of V_C for the KaoS and E866 data are higher than those reported by their respective collaborations [14, 16, 30]. There is some covariance between V_C and R_i, thus our R_i values are also slightly lower than those reported by KaoS and E866. The V_C and R_i values we find using the effective Coulomb potential are reported in Table I. We observe a monotonic decrease in V_C and a monotonic increase in R_i as $\sqrt{s_{NN}}$ increases.

The total charge of the interaction region is determined by the number of participating protons and the degree of stopping for a given collision energy. All of the data considered are either from central Au+Au collisions or central Pb+Pb collisions, therefore the data sets correspond to pion emission from sources with similar number of participating nucleons (estimates range from 312 [29] to 366 [52] participating nucleons) and similar initial overlap volume. With a static source, the Coulomb potential is determined by the source charge distribution and the emission point of the pion. In this simplistic model, the monotonic decrease in V_C seen in the top panel of Fig. 3 would correspond to an increase in the emission radius with increasing beam energy or a reduction in the net charge of the equilibrated system. For all beam energies, the interaction region is first defined by the overlap of the two colliding nuclei. A larger source size would imply

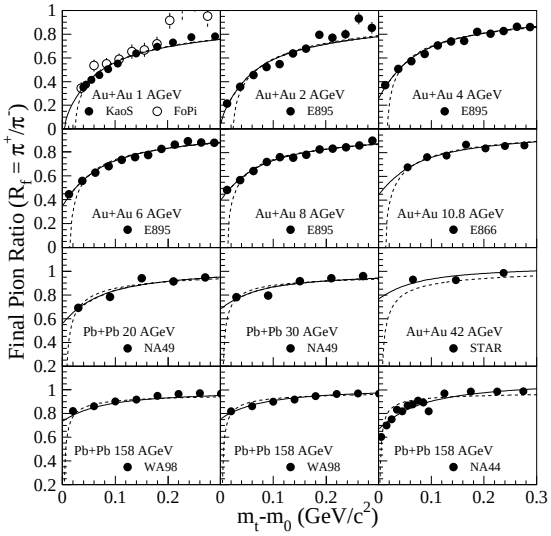

FIG. 2. The mid-rapidity π^+/π^- ratio as a function of $m_t - m_0$ is shown for central Au+Au and Pb+Pb collisions at 1.0 [13, 14], 2.0 [20], 4.0 [20], 6.0 [20], 8.0 [20], 10.8 [16], 20 [28], 30 [28], 42 [29], and 158 [21–23, 26] AGeV. Note that there are two panels for the WA98 data as they report results independently for the two arms of their spectrometer. The ratios are fit with the function given in Eqn. (2). The two curves correspond to use of either a fixed V_C (dashed) or $V_{\rm eff}$ as given in Eqn. (4) (solid).

that there had to have been a period of expansion of the source prior to freeze-out, which negates the overly simplistic static model. Indeed, there is much evidence that heavy-ion collisions create an expanding source which can be characterized by both radial and longitudinal flow velocities. The reduction in V_C with beam energy is related to changes in both the size and the shape of the charge distribution at freeze-out. However, the reduction in the V_C could also indicate that there was less net-charge in the interaction region due to a reduction in the baryon stopping with increased beam energy. To address this point, we have displayed the mid-rapidity net-proton dN/dy values scaled by the number of participating nucleons in the same top panel of Fig. 3 which also shows the V_C values. Since we are concerned with the charge of the interaction region, we subtract the anti-proton $\mathrm{d}N/\mathrm{d}y$ from proton $\mathrm{d}N/\mathrm{d}y$ to get the net-proton values. These net-proton $\mathrm{d}N/\mathrm{d}y$ values are empirically fit with an exponential function which roughly describes

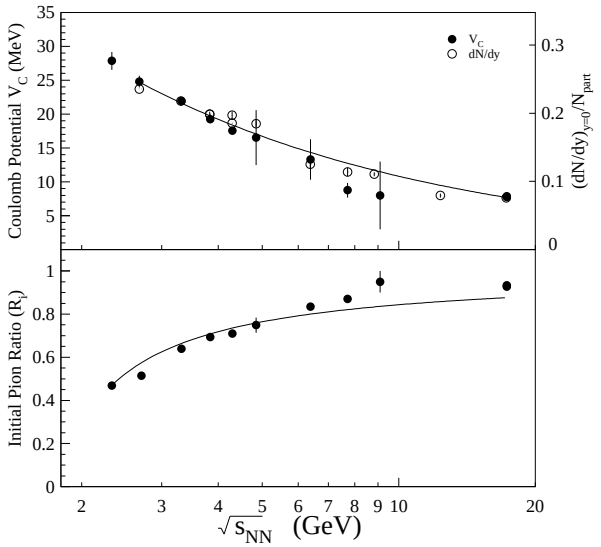

FIG. 3. The top panel shows in solid symbols the Coulomb potential (V_C) extracted from the fits to the pion ratio data shown in Fig. 2 as a function of center-of-mass energy ($\sqrt{s_{NN}}$). In open symbols the normalized net-proton rapidity densities are shown, $(\mathrm{d}N/\mathrm{d}y)_{y=0}/N_{part}$; their axis label is on the right-hand side. The curve in this panel is an empirical fit to the net-proton $\mathrm{d}N/\mathrm{d}y$ data. The proton rapidity density results are from references [29, 47, 49, 51, 52]. The lower panel shows the initial pion ratio, (R_i), extracted from the pion ratio fits as a function of center-of-mass energy. The fit to the data illustrates a smooth transition from pion production exclusively through the Δ resonance channel at the lowest collision energies to thermal production at the highest energies.

the trend. The V_C values track the decrease in net-proton dN/dy. This suggests that the V_C is primarily measuring the charge of the net-charge of the interaction region and the implication is that the emission radius remains unchanged across the range of bombarding energies considered. This final conclusion is consistent with the trends observed for the sidewards pion source radius (R_{side}) as measured in two-pion femtoscopy. In those femtoscopy studies, R_{side} is observed to be approximately 5 fm for all $\sqrt{s_{NN}}$ from 2.5 to 200 GeV [55].

The monotonic increase in the initial pion ratio, R_i, with beam energy seen in the lower panel of Fig. 3 suggests a change in the pion production mechanism. At the lowest reported energies, R_i is slightly below 0.5. This ratio value is expected if all pions were created in first-chance nucleon-nucleon collisions that proceeded through the Δ resonance. This value is determined by the neutron-to-proton ratio in the the central interaction regions of Au+Au collisions. From the numbers of participating protons and neutrons, the relative numbers of pp, np, and nn collisions can be calculated. As the cross sections for the various $N + N \rightarrow N + N' + \pi$ channels are known [41], one can calculate the expected π^+/π^- ratio. From Glauber Monte Carlo models using $\sigma_{NN} =$ 45 mb (which is applicable for center-of-mass energies around 2.5 GeV), we estimate that for the 0-5% central Au+Au data there should be 136 and 218 participating protons and neutrons respectively. Using the pion production cross sections from [41], we estimate a π^+/π^- ratio of 0.47. It is also possible to estimate the relative yields of π^+ and π^-, assuming that all pions are created though an intermediary Δ resonance. Using the isospin of the initial and final states, one can calculate the relative production ratios for the various charge states of the Δ resonance and the relative decay ratios of the Δ^+ and the Δ^0. Using the same number of participating protons and neutrons indicated above and the analysis which exclusively requires production through Δ resonance channel in first chance collisions, we expect an R_i of 0.46. Both of these methodologies reproduce the R_i value extracted using the pion spectra from SIS [14, 15] at 1 AGeV ($\sqrt{s_{NN}} = 2.33$) suggesting that π production proceeds primarily through the Δ resonance at this energy.

The increase in R_i with beam energy suggests that an increasingly larger fraction of pions are formed in isospin independent direct production. Direct production of pion pairs would lead to an equal number of π^+ and π^-. This conjecture is illustrated by the curve in the lower panel of Fig. 3. The curve assumes that the cross sections for π production through the Δ channel remain unchanged with $\sqrt{s_{NN}}$. For center-of-mass energies above 2.33 GeV, the cross section for π pair production ($\sigma_{NN\rightarrow NN\pi^+\pi^-}$) is linearly proportional to ($\sqrt{s_{NN}}$-2.33) GeV. The functional form of the curve is given by:

$$f(x) = \frac{0.47 + A(log(x) - log(2.33))}{1.0 + A(log(x) - log(2.33))} \qquad (6)$$

where the numerator represents the yield π^+, the denominator the yield of π^-, x is the $\sqrt{s_{NN}}$, and A is the slope of the isospin dependent pion production. The qualitative agreement between the curve and the observed R_i values suggests that production through isospin independent channels becomes increasingly important with collision energy.

III. CONCLUSIONS

We have presented a comprehensive study of the low $m_t - m_0$ pion ratios for central Au+Au and Pb+Pb collisions from 1 to 158 AGeV. The spectra and ratios are

fit using a model that accounts for the Coulomb potential of the source including the effects of the pion emission functions and the radial expansion of the source. The addition of the expansion term gives an effective Coulomb potential which improves the fit for the lowest $m_t - m_0$ data points. At mid-rapidity, V_C falls and R_i rises monotonically with bombarding energy. The Coulomb potential is found to be consistent with a reduction in the net-charge of the source due to the reduction in stopping as the beam energy is increased, while the rise in the initial pion ratio suggests that the isospin effects become less important.

This work was supported in part by the US National Science Foundation under Grant No. PHY-1068833.

[1] W. Benenson *et al.*, Phys. Rev. Lett. **43**, 683 (1979).
[2] K. Wolf *et al.*, Phys. Rev. Lett. **42**, 1448 (1979).
[3] S. Nagamiya *et al.*, Phys. Rev. C **24**, 971 (1981).
[4] K. Wolf *et al.*, Phys. Rev. C **26**, 2572 (1982).
[5] M. Gonin *et al.* (E802/E866 Collaboration), Nucl. Phys. A **566**, 601c (1994).
[6] F. Videbaek *et al.* (E866 Collaboration), Nucl. Phys. A **590**, 249c (1995).
[7] K. Libbrecht and S. Koonin, Phys. Rev. Lett. **43**, 1581 (1979).
[8] G. Bertsch, Nature **283**, 280 (1980).
[9] M. Gyulassy and S. Kauffmann, Nucl. Phys. A **362**, 503 (1981).
[10] R. Stock, Phys. Rep. **135**, 259 (1986).
[11] B. Li, Phys. Lett. B **346**, 5 (1995).
[12] M. B. T. Osada, S. Sano and G. Wilk, Phys. Rev. C **54**, 54 (1996).
[13] D. Pelte *et al.* (FoPi Collaboration), Z. Phys. A **357**, 215 (1997).
[14] A. Wagner *et al.* (KaoS Collaboration), Phys. Lett. B **420**, 20 (1998).
[15] W. Reisdorf *et al.* (FoPi Collaboration), Nucl. Phys. A **781**, 459 (2007).
[16] L. Ahle *et al.* (E866 Collaboration), Nucl. Phys. A **610**, 139c (1996).
[17] L. Ahle *et al.* (E802 Collaboration), Phys. Rev. C **57**, 466 (1998).
[18] L. Ahle *et al.* (E866 and E917 Collaborations), Phys. Lett. B **476**, 1 (2000).
[19] J. Barrette *et al.* (E877 Collaboration), Phys. Rev. C **62**, 024901 (2000).
[20] J. Klay *et al.* (E895 Collaboration), Phys. Rev. C **68**, 054905 (2003).
[21] H. Boggild *et al.* (NA44 Collaboration), Phys. Lett. B **372**, 339 (1996).
[22] F. Retière *et al.* (WA98 Collaboration), Nucl. Phys. A **681**, 149c (2001).
[23] L. Rosselet *et al.* (WA98 Collaboration), Nucl. Phys. A **698**, 647c (2002).
[24] M. Aggarwal *et al.* (WA98 Collaboration), Phys. Rev. C **67**, 014906 (2003).
[25] M. Aggarwal *et al.* (WA98 Collaboration), Eur. Phys. J. C **48**, 343 (2006).
[26] I. Beardon *et al.* (NA44 Collaboration), Phys. Rev. C **66**, 044907 (2002).
[27] S. Afanasiev *et al.* (NA49 Collaboration), Phys. Rev. C **66**, 054902 (2002).
[28] C. Alt *et al.* (NA49 Collaboration), Phys. Rev. C **77**, 024903 (2008).
[29] B. Abelev *et al.* (STAR Collaboration), Phys. Rev. C **81**, 024911 (2010).
[30] C. Muntz (E866 and KaoS Collaborations), Acta Polon. B **29**, 3253 (1998).
[31] O. Chvaĺa (NA49 Collaboration), Nucl. Phys. A **749**, 304c (2005).
[32] A. Rybiki and A. Szczurek, Phys. Rev. C **75**, 054903 (2007).
[33] G. Baym and P. Braun-Munzinger, Nucl. Phys. A **610**, 286c (1996).
[34] M.-H. Mostafa and C.-Y. Wong, Phys. Rev. C **51**, 2135 (1995).
[35] S.Teis *et al.*, Z. Phys. A **359**, 297 (1997).
[36] J. G. H. Barz, J.P. Bondorf and H. Heiselberg, Phys. Rev. C **56**, 1553 (1997).
[37] J. G. H. Barz, J.P. Bondorf and H. Heiselberg, Phys. Rev. C **57**, 2536 (1998).
[38] A. Ayala and J. Kapusta, Phys. Rev. C **56**, 407 (1997).
[39] S. J. A. Ayala and J. Kapusta, Phys. Rev. C **59**, 3324 (1999).
[40] F. Zhao-Qing and J. Gen-Ming, Chin. Phys. Lett. **26**, 062501 (2009).
[41] B. VerWest and R. Arndt, Phys. Rev. C **25**, 1979 (1982).
[42] H. S. H. Sorge and W. Greiner, Nucl. Phys. A **498**, 567c (1989).
[43] H. Sorge, Phys. Rev. C **49**, R1253 (1994).
[44] J. Barrette *et al.* (E814 Collaboration), Phys. Lett. B **351**, 93 (1995).
[45] N. Herrmann *et al.* (FoPi Collaboration), Nucl. Phys. A **610**, 49c (1996).
[46] W. Reisdorf *et al.* (FoPi Collaboration), Nucl. Phys. A **848**, 366 (2010).
[47] J. Klay *et al.* (E895 Collaboration), Phys. Rev. Lett. **88**, 102301 (2002).
[48] B. Back *et al.* (E917 Collaboration), Phys. Rev. Lett. **86**, 1970 (2001).
[49] B. Back *et al.* (E917 Collaboration), Phys. Rev. C **66**, 054901 (2002).
[50] L. Ahle *et al.* (E802 Collaboration), Phys. Rev. C **59**, 2173 (1999).
[51] L. Ahle *et al.* (E802 Collaboration), Phys. Rev. C **60**, 064901 (1999).
[52] C. Alt *et al.* (NA49 Collaboration), Phys. Rev. C **73**, 044910 (2006).
[53] T. Anticic *et al.* (NA49 Collaboration), Phys. Rev. C **83**, 014901 (2011).
[54] J. S. E. Schnedermann and U. Heinz, Phys. Rev. C **48**, 2462 (1993).
[55] L. Adamczyk *et al.* (STAR Collaboration), (2014), Phys. Rev. C (submitted) Archives (1403.4972).